BIOCHEMISTRY
including biophysical chemistry & molecular biology

Article

pubs.acs.org/biochemistry

Major Groove Binding Track Residues of the Connection Subdomain of Human Immunodeficiency Virus Type 1 Reverse Transcriptase Enhance cDNA Synthesis at High Temperatures

Tania Matamoros, Verónica Barrioluengo, David Abia, and Luis Menéndez-Arias*

Centro de Biología Molecular "Severo Ochoa", Consejo Superior de Investigaciones Científicas-Universidad Autónoma de Madrid, 28049 Madrid, Spain

Supporting Information

ABSTRACT: At high temperatures, RNA denaturation can improve the efficiency and specificity of reverse transcription. Refined structures and molecular models of HIV-1 reverse transcriptases (RTs) from phylogenetically distant clades (i.e., group M subtype B and group O) revealed a major interaction between the template-primer and the Arg^{358}-Gly^{359}-Ala^{360} triad in the large subunit of HIV-1$_{M/B}$ RT. However, fewer contacts were predicted for the equivalent Lys^{358}-Ala^{359}-Ser^{360} triad of HIV-1$_O$ RT and the nucleic acid. An engineered HIV-1$_O$ K358R/A359G/S360A RT showed increased cDNA synthesis efficiency above 68 °C, as determined by qualitative and quantitative reverse transcription polymerase chain reactions. In comparison with wild-type HIV-1$_O$ RT, the mutant enzyme showed higher thermal stability but retained wild-type RNase H activity. Mutations that increased the accuracy of HIV-1$_{M/B}$ RTs were tested in combination with the K358R/A359G/S360A triple mutation. Some of them (e.g., F61A, K65R, K65R/V75I, and V148I) had a negative effect on reverse transcription efficiency above 65 °C. RTs with improved DNA binding affinities also showed higher cDNA synthesis efficiencies at elevated temperatures. Two of the most thermostable RTs (i.e., mutants T69SSG/K358R/A359G/S360A and K358R/A359G/S360A/E478Q) showed moderately increased fidelity in forward mutation assays. Our results demonstrate that the triad of Arg^{358}, Gly^{359}, and Ala^{360} in the major groove binding track of HIV-1 RT is a major target for RT stabilization, and most relevant for improving reverse transcription efficiency at high temperatures.

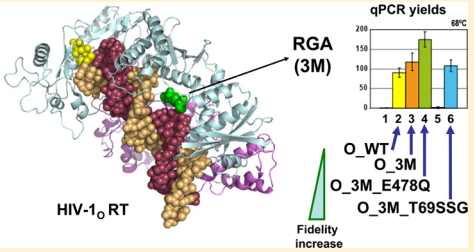

Reverse transcriptases (RTs) are enzymes responsible for the replication of the viral genome. The RNA-dependent DNA polymerase, ribonuclease H, and DNA-dependent DNA polymerase activities of the RT are essential for the transcription of the viral RNA to produce double-stranded DNA that can be integrated into the host genome.[1,2] RTs are widely used in a number of research applications aimed at studying transcriptomics and gene expression analysis. Examples are end point and quantitative reverse transcription polymerase chain reaction (RT-PCR), microarray analysis, complementary DNA (cDNA) cloning, and next-generation RNA sequencing.[3−7] Frequently used RTs are the polymerases of avian myeloblastosis virus (AMV) and murine leukemia virus (MLV).

A major obstacle in cDNA synthesis is the presence of RNA secondary structures in the template that slow or even halt the RT reaction.[8,9] AMV RT can be used to copy mRNA at temperatures higher than those of MLV RT, but its use is limited by its lower yield and higher RNase H activity.[10] Mutations that eliminate the RNase H activity of oncoretroviral RTs (e.g., D524A, D524G, E562Q, or D583N in MLV RT and D450A in AMV RT) increase their stability at elevated temperatures.[11−13] Those effects have been attributed to the increased template-primer binding affinity of RNase H-deficient RTs.[11] High-throughput screening and *in vitro* evolution studies have selected for mutant MLV RTs that showed an increased half-life at 55 °C and a greater efficiency of cDNA synthesis at high temperatures.[14,15] The RTs with the highest thermostability had combinations of mutations such as E69K, E302R, W313F, L435G, and N454K[14] or L139P, D200N, T330P, L603W, and E607K[15] that promoted tighter binding to the template-primer. However, structural analysis of the DNA polymerase domain (residues 28−487) of xenotropic murine leukemia virus-related virus (XMRV) RT bound to an RNA−DNA hybrid showed that most of the substituted amino acids in the thermostable MLV RTs were located some distance away from the template-primer.[16] Among them, Glu^{302} was the only mutated residue involved in interactions with the nucleic acid.

Recombinant human immunodeficiency virus type 1 (HIV-1) RTs derived from group M subtype B clones (e.g., BH10 and HXB2) have been studied extensively but have not been used as a tool to copy mRNA because of their relatively high error rate compared to those of AMV and MLV RTs.[17] However, wild-type (WT) HIV-1$_{M/B}$ BH10 strain RT shows higher activity and half-life than the MLV RT at temperatures in the range from 50 to 60 °C.[18] Compared to the BH10

Received: October 10, 2013
Revised: December 3, 2013
Published: December 4, 2013

polymerase, a WT HIV-1 RT derived from the phylogenetically distant clade group O showed increased stability in the presence of urea[19] and higher efficiency in RT-PCRs when cDNA synthesis was performed at temperatures as high as 68 °C.[18] Although the HIV-1 group O (HIV-1_O) RT is ∼6-fold less accurate than the MLV RT,[20,21] it is more faithful than the HIV-$1_{M/B}$ (BH10) polymerase and less prone to introduction of deletions and insertions than AMV and MLV RTs.[17,18,22,23]

HIV-1 RTs are heterodimers composed of subunits of 66 and 51 kDa (i.e., p66 and p51, respectively). Crystal structures of HIV-$1_{M/B}$ RTs revealed that both subunits contain four common subdomains (fingers, palm, thumb, and connection), while the RNase H domain is found only in p66. The template-primer interacts with residues of the DNA polymerase and RNase H domains of p66, as well as with the thumb and connection subdomains of p51. Interactions that stabilize the RT heterodimer or its binding to nucleic acid have been determined from crystal structures of HIV-$1_{M/B}$ RT and a molecular model of HIV-1_O RT built on the basis of the structure of the ternary complex of HIV-$1_{M/B}$ RT, double-stranded DNA (dsDNA), and dTTP.[24] Free energy interaction matrices were used to identify relevant residues in HIV-$1_{M/B}$ and HIV-1_O RTs that contribute to template-primer binding. By making the relevant substitutions in the connection subdomain of HIV-1_O RT, we have obtained enzymes with increased nucleic acid binding affinity and enzymes that are more efficient than the WT RT in reverse transcription reactions conducted at elevated temperatures.

EXPERIMENTAL PROCEDURES

Molecular Modeling. The HIV-1_{ESP49} group O RT model was built by standard homology modeling techniques using MODELER version 9.7.[25] The structure of the ternary complex of HIV-1_{HXB2} RT, dsDNA, and dTTP (Protein Data Bank entry 1RTD)[24] was used as a template. The molecular model and the crystal structure were hydrated by using boxes containing explicit water molecules, energy minimized, heated (20 ps), and equilibrated (100 ps). Then, when the equilibration was reached, molecular dynamics trajectories were continued for 20 ns. Structures were homogeneously sampled every 40 ps and stored for postprocessing. All the simulations were performed at constant pressure (1 atm) and temperature (300 °K) with an integration time step of 2 fs. The SHAKE algorithm[26] was used to constrain all the bonds involving H atoms at their equilibrium distances. Periodic boundary conditions and the particle mesh Ewald methods were applied to treat long-range electrostatic effects.[27] AMBER ff03[28] and TIP3P[29] force fields were used in all cases. Finally, the effective binding free energies were estimated with the MM-GBSA[30] approach that calculates the free energy of binding as a sum of a molecular mechanics (MM) interaction term, a solvation contribution through a generalized Born (GB) model, and a surface area (SA) contribution to account for the nonpolar part of the desolvation. A 12-6 Lennard-Jones term was used to model the MM contribution. For GB, the solute dielectric constant was set to 4, whereas that of the solvent was set to 80. The dielectric boundary was calculated using a solvent probe radius of 1.4 Å. The SA contribution was approximated as a linear relationship to the change in solvent accessible surface area (SASA). All the trajectories and analysis were performed using the AMBER 10 computer program and associated modules.[31] Free energy decomposition interaction matrices, obtained from the same snapshots, were represented in an energy-dependent color gradient using Matrix2png.[32]

Mutagenesis, Expression, and Purification of Recombinant RTs. Site-directed mutagenesis was conducted with the QuikChange site-directed mutagenesis kit (Stratagene) by following the manufacturer's instructions and using the mutagenic primers listed in Table S1 of the Supporting Information. Plasmid p66RTB containing the WT RT-coding sequence of an HIV-1_{ESP49} group O isolate[19] was used as a template to introduce the K28E mutation or the K358R, A359G, and S360A mutations (designated 3M). Additional changes were introduced in a sequential manner into derivatives of p66RTB(O_WT) containing the 3M cluster of mutations. After mutagenesis, the entire RT-coding regions were sequenced and, if correct, used for RT expression and purification. RT p66 subunits carrying a His_6 tag at the C-terminus were coexpressed with the HIV-1 protease using the *Escherichia coli* XL1 Blue strain, and the obtained p66−p51 heterodimers were then purified by ionic exchange followed by immobilized metal affinity chromatography on Ni^{2+}-nitrilo-acetic acid agarose.[18,33] Enzymes were quantified by active-site titration before biochemical studies.[34]

DNA Polymerase and RNase H Activity Assays. DNA polymerase activity assays were conducted at 37 °C in 50 mM Tris-HCl (pH 8.0) buffer, containing 20 mM NaCl, 10 mM $MgCl_2$, 8 mM dithiothreitol, 50 μM [^{3}H]dTTP, and 1 μM poly(rA)/oligo(dT)$_{16}$, as previously described.[20] RT thermal stabilities were determined by measuring the residual RNA-dependent DNA polymerase activity, after preincubating the enzyme and the template-primer in reaction buffer for 0−60 min at 50 °C.[20] Polymerization reactions were initiated by adding buffer containing [^{3}H]dTTP. The active RT concentration in these assays was kept around 20 nM. RNase H activities were determined with a 31/21-mer RNA−DNA complex as described previously.[18]

Reverse Transcription PCR Assays. A two-step RT-PCR assay was used to determine the efficiency of the reverse transcription reaction at different temperatures.[18] Reverse transcription reactions (20 μL) were conducted in 50 mM Tris-HCl (pH 8.3), containing 75 mM KCl, 3 mM $MgCl_2$, 10 mM dithiothreitol, 1 unit/μL RNase inhibitor (RNasin Plus, Promega), dATP, dCTP, dGTP, and dTTP (500 μM each), 5 μM oligo(dT)$_{16}$, 50 ng/μL mouse liver RNA (Stratagene), and the corresponding RT at 150 nM (active-site concentration). The RNA template and the oligo(dT)$_{16}$ primer were annealed by preincubation at 68 °C for 3 min and then slowly cooled at room temperature. The cDNA synthesis reactions were conducted at different temperatures (within the range of 37−78 °C) for 60 min and then stopped when the mixtures were heated at 92 °C for 10 min. DNA amplifications were conducted as previously described using the Expand High Fidelity DNA polymerase mix (Roche).[18] The used PCR primers were 5′-CCTAGGCACCAGGGTGTGAT-3′ (ACT1), 5′-CGGTCAGGATCTTCATGAGG-3′ (ACT2), and 5′-CGTACTCCTGCTTGCTGATCC-3′ (ACT3).

Quantitative Real-Time PCR Assay. Reverse transcription reactions were conducted as described above. The cDNA synthesis yields of β-actin and glyceraldehyde-3-phosphate dehydrogenase (GAPDH) mRNAs were measured after amplification with primers 5′-CTAAGGCCAACCGTGAAAAG-3′ and 5′-ACCAGAGGCATACAGGGACA-3′ for β-actin and 5′-CTCCCACTCTTCCACCTTCG-3′ and 5′-CATACCAGGAAATGAGCTTGACAA-3′ for GAPDH, using SYBR

dx.doi.org/10.1021/bi401390x | *Biochemistry* 2013, 52, 9318−9328

Green I detection chemistry. Briefly, qPCRs (10 μL) were performed in triplicate. Each reaction mixture contained the amount of cDNA equivalent to 5 ng of total RNA, each primer at 250 nM, and 5 μL of Power Sybr Green PCR Master Mix (Applied Biosystems, product no. 4367659), which includes AmpliTaq Gold DNA polymerase, dNTPs, and the rest of the reagents required to complete the PCR amplification. Real-time PCR was performed in an Applied Biosystems 7900HT instrument, using MicroAmp Optical 384-well reaction plates with barcode. The cycling protocol included after an initial denaturation at 95 °C for 10 min, a series of 40 two-step cycles (15 s at 95 °C and 1 min at 60 °C). A melting curve from 60 to 95 °C (2% ramp) at the end of the program was included to verify the specificity of the amplification reaction. Fluorescence was acquired during the 60 °C and melting steps. All samples were run in the same plate with negative controls and primer efficiency curves for each gene amplification.

Data were analyzed with the qPCR quantification software SDS version 2.2.1 (Applied Biosystems). The threshold cycle (C_T) in which the fluorescence significantly exceeds background was determined by the quantification software. The linearity in cDNA synthesis was determined by performing qPCR assays over a six-point 1:4 dilution curve made with a pooled cDNA sample containing amounts equivalent to 0.05−50 ng of RNA. C_T values obtained in all experiments were within the ranges validated by the dilution curves. Amplification efficiencies were determined as fold differences relative to data obtained with WT HIV-1_{BH10} RT under the same conditions.[4,35] ΔC_T was calculated for each sample with the equation $\Delta C_T = C_T - C_{Tref}$. C_T and C_{Tref} are the average threshold cycles obtained for the analyzed RT variant and the reference HIV-1_{BH10} RT, respectively, in assays conducted under the same conditions. Relative yields were then calculated as $2^{\Delta C_T}$ for each cDNA. Results are expressed as means ± the standard deviation of $2^{\Delta C_T}$ of the three replicates obtained for each RT and temperature.

DNA Binding Affinity. Dissociation equilibrium constants (K_d) for RTs and DNA−DNA complexes were obtained with the template-primer D38/25PGA by following a previously described procedure.[36] Briefly, RTs (at ∼3 nM) were preincubated at 37 °C with increasing concentrations of the 5′-^{32}P-labeled template-primer (2−60 nM) in 10 μL of 100 mM Hepes (pH 7.0) buffer, containing 30 mM NaCl, 30 mM magnesium acetate, 130 mM potassium acetate, 1 mM dithiothreitol, and 5% polyethylene glycol. Reactions were initiated by adding 10 μL of a solution containing 130 mM potassium acetate, 1 mM dithiothreitol, 5% polyethylene glycol, and 1 mM dTTP. Aliquots of 4 μL were removed at different times, quenched with 4 μL of sample loading buffer, and analyzed by denaturing polyacrylamide electrophoresis. Burst amplitudes (i.e., RT bound to the template-primer at time zero) were plotted against the template-primer concentration in the assay, and the data were fit to a quadratic equation to obtain the equilibrium dissociation constant for the binding of RT to the template-primer.[37]

Mispair Extension Fidelity Assays. Pre-steady-state kinetics of nucleotide incorporation were determined with heteroduplex DNA−DNA 31/21-mers containing matched (G:C) and mismatched 3′ ends (G:T, G:G, and G:A). The kinetic parameters of nucleotide (dTTP) incorporation were obtained with a rapid quench instrument (model QFM-400, Bio-Logic Science Instruments, Claix, France), upgraded with a mixer cross and a special mixer (Bio-Logic) that facilitate the determination of catalytic rate constants of >20 s^{-1}. Reactions were conducted in 50 mM Tris-HCl (pH 8.0) containing 50 mM KCl and 18 mM $MgCl_2$. The concentration of the template-primer in the mixture was 100 nM, and the RT was supplied at a concentration of 50 nM (active sites) except for reactions involving extensions of G:T, G:G, and G:A mispairs. In these cases, the enzyme was supplied at a concentration of 120 nM to eliminate the influence of the enzyme turnover rate (k_{ss}), which interferes in the measurements of low incorporation rates. Mismatched template-primer concentrations were well above their dissociation equilibrium constants (K_d) for WT and mutant RTs as determined by equilibrium competition assays.[38] Oligonucleotides 31T (5′-TTTTTTTTTAGGATACATATGGTTAAAGTAT-3′) and 21P (5′-ATACTTTAACCATATGTATCC-3′) were used as the template and primer, respectively. Mismatched extension reactions were conducted with derivatives of 21P having T, G, or A at their 3′ ends.

M13mp2 lacZα Forward Mutation Assays. The fidelity of DNA-dependent DNA synthesis was determined using the forward mutation assay,[39] under the previously described conditions.[20,21] Mutant frequencies were calculated as the ratio of mutant (light blue or colorless) plaques to the total number of plaques screened. Mutant phenotypes were confirmed by nucleotide sequencing of the phage replicative-form DNA.[39]

RESULTS

Molecular Models and Mutant Design. The WT RT of the HIV-1_O ESP49 strain (obtained from an untreated patient[19]) has a sequence that is ∼80% identical to that of prototypic HIV-$1_{M/B}$ RTs, such as those derived from strains BH10, HXB2, or NL4-3. On the basis of their similarity, a molecular model of HIV-1_O RT was built by using the structure of WT HIV-$1_{M/B}$ (HXB2 strain) RT bound to double-stranded DNA and dTTP as a template (Figure 1A). The model and the crystal structure were refined by molecular dynamics. The higher stability of HIV-1_O RT relative to that of HIV-$1_{M/B}$ RT was demonstrated *in vitro*.[18,19] Absolute free energies of interaction between p66 and p51 subunits, calculated by using the MM-PBSA method, were similar for both RTs with values of −202.03 ± 12.60 kcal/mol for HIV-$1_{M/B}$ RT and −201.58 ± 12.88 kcal/mol for the HIV-1_O polymerase (Figure S1 of the Supporting Information). In contrast, the predicted affinity for the template-primer was higher in the case of HIV-1_O RT, with free energies of interaction with the DNA complex of −343.43 ± 19.27 kcal/mol in contrast to a value of −277.12 ± 15.96 kcal/mol, as observed in the case of HIV-$1_{M/B}$ RT.

Subunit interactions affect highly conserved residues in HIV-$1_{M/B}$ and HIV-1_O RTs.[19] In both RTs, major interactions occur between residues 52−57 and 136−143 of p51 and residues 85−96 of p66, between amino acids 394−401 of p51 and 358−377 of p66, and between residues 331−392 and 418−424 of p51 and residues 402−410 of p66. Differences between HIV-$1_{M/B}$ and HIV-1_O RTs were detected by comparing the free energy decomposition interaction matrices for both enzymes (Figure S2 of the Supporting Information). Compared with the HIV-1_O RT, the group M subtype B enzyme showed stronger interactions between Lys^{385} (p66) and Glu^{28} (p51), followed by Gln^{370} (p66) and Glu^{396} (p51), and Thr^{409} (p66) and Asp^{364} (p51). Most of those residues were conserved in both RTs, although WT HIV-1_O RT contains Lys instead of Glu at position 28.

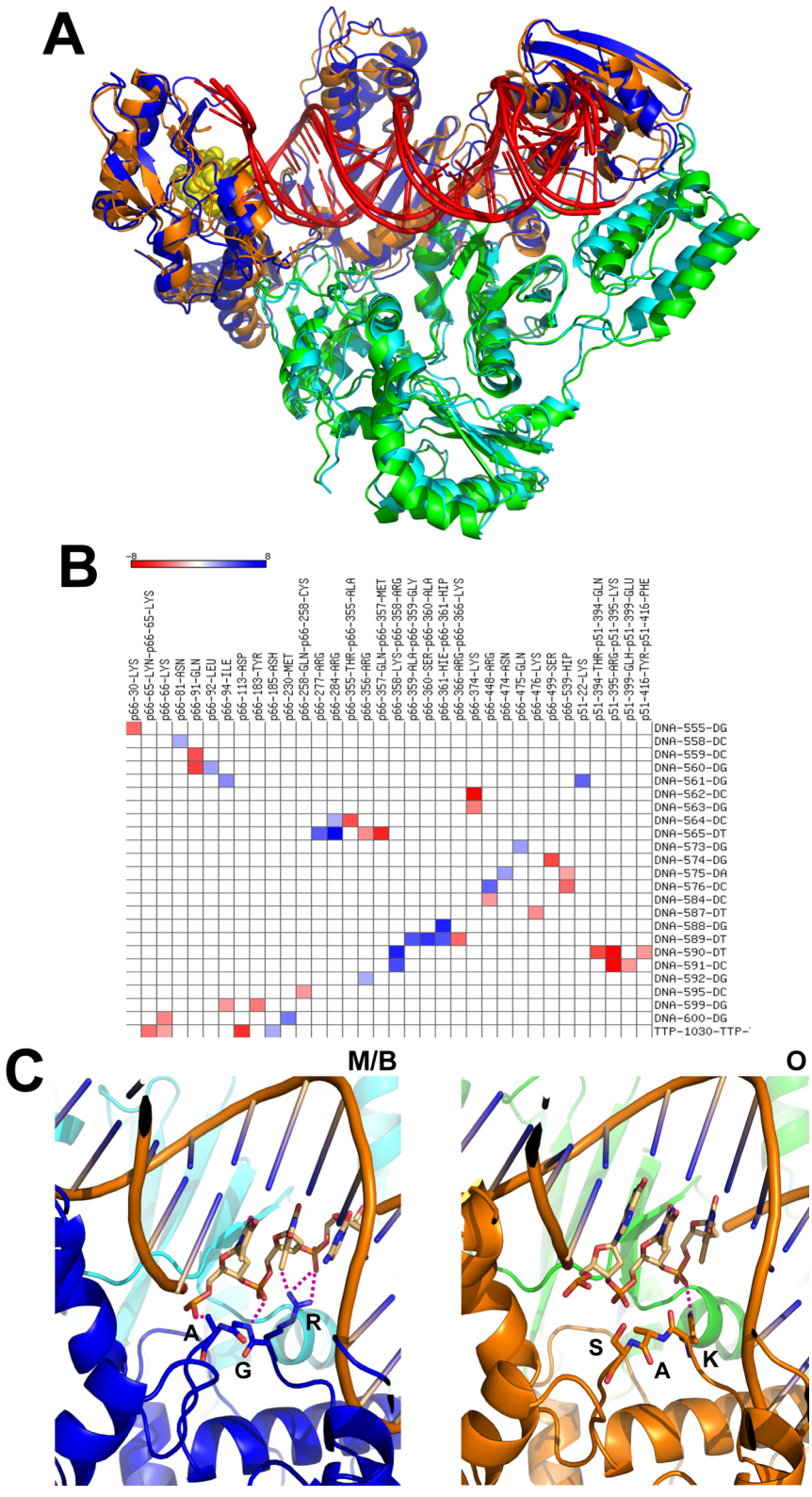

Figure 1. Molecular model of HIV-1_O RT in a ternary complex with double-stranded DNA (dsDNA) and dTTP. (A) Superposition of the modeled structure of the HIV-1_O RT and the crystal structure of HIV-$1_{M/B}$ (HXB2 strain) RT in complex with dsDNA and dTTP (both refined by molecular dynamics). In the HIV-1_O RT model, p66 is colored orange and p51 green. In the HIV-$1_{M/B/HXB2}$ RT structure, the p66 and p51 subunits are colored blue and cyan, respectively. The dsDNA is colored red, and the incoming dTTP is depicted as yellow spheres. (B) Analysis of interactions between the RT and template-primer based on the differences between the free energy decomposition matrices obtained for the ternary structures containing the HIV-$1_{M/B/HXB2}$ and HIV-1_O RTs. Blue boxes represent interactions found to be stronger in the HIV-$1_{M/B/HXB2}$ RT complex, while red squares indicate interaction sites in the HIV-1_O RT that are stronger than in the HIV-$1_{M/B/HXB2}$ RT complex. (C) Cartoon and stick representation of interactions between RT connection subdomain residues 358−360 of HIV-$1_{M/B/HXB2}$ RT (blue) and HIV-1_O RT (orange) and the template-primer (red). Images in panels A and C were generated with the PyMOL Molecular Graphics System, version 1.5.0.4 (Schrödinger, LLC, Portland, OR).

dx.doi.org/10.1021/bi401390x | *Biochemistry* 2013, 52, 9318−9328

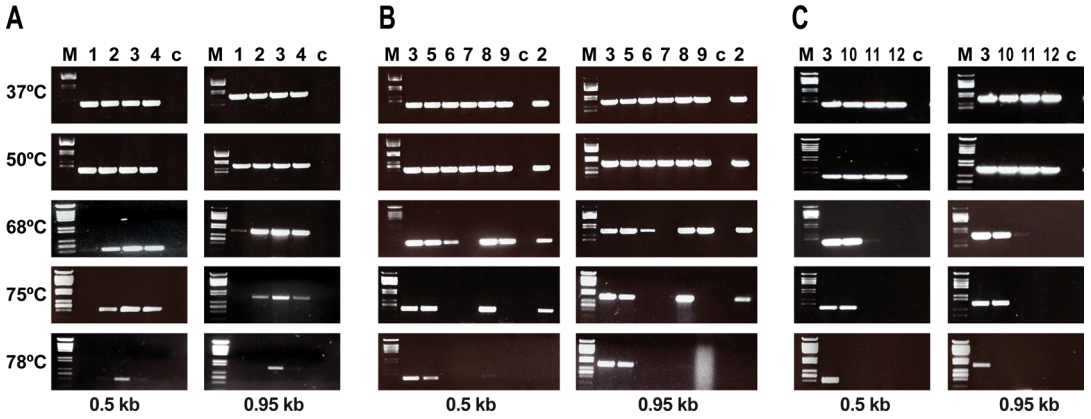

Figure 2. Effect of temperature on cDNA synthesis and two-step reverse transcription PCR. The cDNA synthesis reactions were conducted for 60 min at the indicated temperatures, in a buffer containing 50 ng/μL mouse liver RNA and 150 nM RT (active-site concentration). Reactions were stopped when mixtures were heated at 92 °C for 10 min. The product of the cDNA synthesis reaction was amplified with the Expand High Fidelity DNA polymerase. Amplifications of actin DNA fragments of 0.5 and 0.95 kb are shown. (A) Comparison of reverse transcription efficiencies of BH10_WT (lane 1), O_WT (lane 2), O_3M (lane 3), and O_K28E (lane 4) RTs. (B) Comparison of reverse transcription efficiencies of O_WT (lane 2), O_3M (lane 3), O_5M (lane 5), O_3M_K65R (lane 6), O_3M_K65R/V75I (lane 7), O_3M_E478Q (lane 8), and O_3M_K65R/E478Q (lane 9) RTs. (C) Comparison of reverse transcription efficiencies of O_3M (lane 3), O_3M_T69SSG (lane 10), O_3M_V148I (lane 11), and O_3M_F61A (lane 12) RTs. Lanes M and c show molecular size markers (HindIII digest of phage Φ29 DNA) and a control reaction mixture (conducted without RT), respectively. Results are representative of three independent experiments.

The analysis of interactions with the template-primer revealed that both RTs have major contacts with the nucleic acid around positions 72−94, 255−266, 277−285, 353−361, 448−451, 473−478, and 499−505 of the 66 kDa subunit (Figure S3 of the Supporting Information). Interestingly, in the crystal structure of HIV-$1_{M/B}$ RT bound to dsDNA and dTTP, very strong interactions were detected around positions 284 and 358−361 of p66, while interactions involving residues 374 of p66 and 394−399 of p51 were predicted to be much stronger in HIV-1_O RT. Although Arg^{284} is conserved in both RTs, they show sequence differences at positions 355−361. While the HIV-$1_{M/B}$ RT sequence is Ala^{355}-Arg^{356}-Met^{357}-Arg^{358}-Gly^{359}-Ala^{360}-His^{361}, the equivalent sequence in HIV-1_O RT is Thr^{355}-Arg^{356}-Gln^{357}-Lys^{358}-Ala^{359}-Ser^{360}-His^{361}. Comparison of pairwise interaction energies in this region suggests a stabilizing role for the three residues at positions 358−360 in the HIV-$1_{M/B}$ RT (Figure 1B). Residues 358−360 in the HIV-$1_{M/B}$ RT are approximately 2.7−3.1 Å away from the DNA, while in the predicted HIV-1_O RT structure, the distance increases to 5.3−5.4 Å. A detailed analysis of the interactions affecting those residues reveals the presence of a number of hydrogen bonds in the HIV-$1_{M/B}$ RT structure that connect the major groove of the DNA with the Gly^{359}-Ala^{360} polypeptide backbone and the side chain of Arg^{358} (Figure 1C). Most of these bonds are missing in the HIV-1_O RT model. There is only one, affecting Lys^{358} and the phosphate backbone of the DNA, that is maintained in this structure.

On the basis of the previous analysis, the K28E mutation and the K358R/A359G/S360A combination (designated 3M) were introduced into the WT HIV-1_O RT sequence to improve the RT stability. In addition to the 3M cluster, we also made another mutant HIV-1_O RT that contained the additional changes at positions 355 and 357 (i.e., T355A/Q357M/K358R/A359G/S360A, designated 5M).

Mutational Cluster K358R/A359G/S360A Increases the Efficiency of HIV-1_O RT in cDNA Synthesis Reactions Conducted at High Temperatures. RT efficiencies at high temperatures were determined for the O_WT enzyme and mutants K28E and K358R/A359G/S360A (i.e., O_3M), using a two-step reverse transcription PCR assay that included an initial cDNA synthesis reaction at a fixed temperature. The amplification of 0.5 and 0.95 kb actin fragments from mouse liver total RNA showed that the K28E substitution had a minimal impact on the reverse transcription efficiency at temperatures in the range of 37−75 °C (Figure 2A and Figure S4 of the Supporting Information). However, yields were substantially higher with the O_3M RT at 75 and 78 °C. These results were consistent with the higher thermal stability of the mutant enzyme that showed a half-life of 6.01 ± 1.08 min at 50 °C in DNA polymerization assays conducted with poly(rA)/oligo$(dT)_{16}$. In contrast, the half-life of the O_WT RT was 3.45 ± 0.48 min. In addition, we found that the mutant O_3M RT retained approximately 15−21% of its specific DNA polymerase activity after a 30 min incubation at 50 °C, while the activity of the O_WT enzyme was reduced to <10%.

Both RTs showed very similar RNase H cleavage rates, as determined in assays conducted with a 31/21-mer RNA−DNA complex. The obtained k_{obs} values were 2.60 ± 0.26 min^{-1} for the O_WT RT and 2.49 ± 0.15 min^{-1} for the O_3M mutant. Therefore, observed differences in cDNA synthesis efficiencies between both enzymes are independent of their RNase H activity.

Interestingly, the addition of T355A and Q357M to the K358R/A359G/S360A complex had no effect on the efficiency of reverse transcription at all tested temperatures (Figure 2B and Figure S4 of the Supporting Information). The reduced thermal stability of WT HIV-$1_{M/B}$ RT (i.e., BH10 RT) was confirmed in the RT-PCR experiments, because no amplifications were observed in cDNA synthesis reactions conducted with this enzyme above 68 °C (Figure 2A).

We have previously reported that mutation K65R, double mutation K65R/V75I, and mutation E478Q increased the fidelity of DNA synthesis catalyzed by HIV-1_O RT.[20,38] We analyzed the effects of those amino acid changes in combination with triple mutation K358R/A359G/S360A on the reverse transcription efficiency at high temperatures. As shown in Figure 2B (and in Figure S4 of the Supporting Information), all tested combinations (i.e., adding K65R,

dx.doi.org/10.1021/bi401390x | Biochemistry 2013, 52, 9318−9328

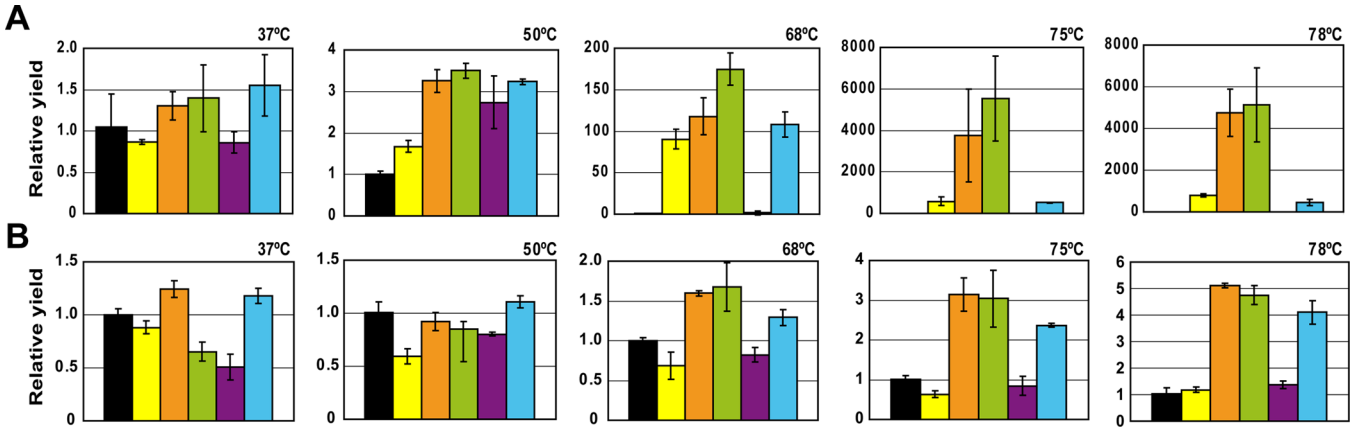

Figure 3. Reverse transcription yields at different temperatures determined by qPCR. Total mouse liver RNA was used as input material. Amplifications of β-actin and GAPDH mRNAs are shown in panels A and B, respectively. Error bars indicate the standard deviation of samples run in quadruplicate. The analyzed RTs were BH10_WT (black), O_WT (yellow), O_3M (orange), O_3M_E478Q (green), O_3M_K65R/V75I (purple), and O_3M_T69SSG (blue). Relative yields refer to the number of cDNA copies (assuming 100% PCR efficiency) produced by the BH10_WT RT.

K65R/V75I, K65R/E478Q, and E478Q) resulted in RTs with decreased efficiency of cDNA synthesis at high temperatures. The destabilizing effects were larger for K65R/V75I and less prominent in the case of the RNase H-inactivating mutation E478Q. Other amino acid substitutions that increase the accuracy of HIV-1 RT without compromising its DNA polymerase activity at 37 °C are F61A and V148I, as well as insertion T69SSG (i.e., substitution T69S and insertion of the Ser-Gly dipeptide).[40−43] F61A, V148I, and the insertion complex (T69SSG) reduced the efficiency of the cDNA synthesis reaction upon being added to the K358R/A359G/S360A complex. However, the loss of activity at temperatures in the range of 68−78 °C was more pronounced for the RTs containing the F61A or the V148I mutation (Figure 2C and Figure S4 of the Supporting Information).

Quantitative Analysis of the Reverse Transcription Efficiency and Template-Primer Binding Affinities of Engineered RTs. The RT-PCR studies and polymerase half-life measurements at 50 °C showed that the three connection subdomain mutations K358R, A359G, and S360A were sufficient to produce a large increase in thermal stability. All amino acid substitutions that were previously characterized as antimutators had a negative effect on the thermal stability of the O_3M RT. However, this effect was relatively minor for T69SSG and E478Q and most evident in the case of K65R/V75I. Reverse transcription yields rendered by these enzymes in comparison with those of the O_WT and BH10_WT RTs were estimated by qPCR at different temperatures, based on the amplification of housekeeping gene mRNAs such as those of β-actin and glyceraldehyde-3-phosphate dihydrogenase (GAPDH) (Figure 3). In the case of β-actin, differences at 37 °C were relatively small (<2-fold). At 50 °C, the four mutants containing changes at positions 358−360 showed the highest yields, with efficiencies that were 2−3-fold higher than those obtained for O_WT and BH10_WT RTs (Figure 3A and Figure S5 of the Supporting Information).

These differences were dramatically increased at higher temperatures. At 75 and 78 °C, mutants O_3M and O_3M_E478Q (i.e., K358R/A359G/S360A/E478Q) were the most efficient, with yields that were 4000−6000 times larger than those obtained with the BH10_WT RTs. The differences in relative yields were smaller for the amplification of the GAPDH gene (Figure 3B). Thus, at temperatures in the range of 37−68 °C, differences were relatively small (Figure S5 of the Supporting Information). However, results were in good agreement with those obtained for the β-actin gene, because both O_3M and O_3M_E478Q RTs, together with the O_3M_T69SSG (i.e., T69SSG/K358R/A359G/S360A) mutant, were found to be the most efficient at the highest temperatures tested (i.e., 75 and 78 °C).

The dissociation equilibrium constants for WT and mutant HIV-1 RTs and heteropolymeric template-primers are listed in Table 1. The triad of mutations in the connection subdomain (i.e., K358R, A359G, and S360A) produced a 3-fold increase in nucleic acid binding affinity. However, further addition of mutations at positions 355 and 357 had a minor effect on the apparent K_d. Interestingly, RTs showing the highest cDNA synthesis efficiency above 68 °C (i.e., O_3M_E478Q and

Table 1. Dissociation Equilibrium Constants for WT and Mutant HIV-1 RTs and DNA−DNA Template-Primers[a]

RT	apparent K_d (nM)
BH10_WT	5.84 ± 1.67
O_WT	4.57 ± 0.51
O_K28E	4.50 ± 1.52
O_3M	1.52 ± 0.60
O_5M	2.04 ± 0.39
O_3M_K65R	2.56 ± 0.75
O_3M_K65R/V75I	3.34 ± 0.65
O_3M_E478Q	1.58 ± 0.67
O_3M_K65R/E478Q	7.22 ± 1.86
O_3M_F61A	8.64 ± 1.21
O_3M_V148I	3.52 ± 0.76
O_3M_T69SSG	1.81 ± 0.44

[a]3M and 5M stand for the combinations of mutations K358R, A359G, and S360A and mutations T355A, Q357M, K358R, A359G, and S360A, respectively. The K_d values were determined at 37 °C using the template-primer D38/25PGA (sequences given below). Reported values are averages ± standard deviations obtained from at least three independent experiments.

```
D38      5´ GGGTCCTTTCTTACCTGCAAGAATGTATAGCCCTACCA 3´
25PGA    3´           GGACGTTCTTACATATCGGGATGGT 5´
```


dx.doi.org/10.1021/bi401390x | Biochemistry 2013, 52, 9318−9328

Table 2. Pre-Steady-State Kinetic Parameters for Mispair Extension[a]

RT	base pair at the 3′ end[b]	k_{pol} (s^{-1})	K_d (μM)	k_{pol}/K_d (μM^{-1} s^{-1})	mismatch extension ratio (f_{ext})[c]
O_WT	G:C	32.3 ± 1.5	11.4 ± 1.7	2.83 ± 0.43	
	G:T	13.8 ± 2.8	8148 ± 3206	(1.70 ± 0.75) × 10^{-3}	(6.00 ± 2.80) × 10^{-4}
	G:G	0.56 ± 0.07	1132 ± 316	(4.94 ± 1.51) × 10^{-4}	(1.74 ± 0.59) × 10^{-4}
	G:A	0.021 ± 0.003	7817 ± 2334	(2.71 ± 0.89) × 10^{-6}	(9.57 ± 3.46) × 10^{-7}
O_3M	G:C	16.4 ± 0.6	5.0 ± 0.7	3.28 ± 0.50	
	G:T	13.5 ± 1.3	7615 ± 1519	(1.77 ± 0.39) × 10^{-3}	(5.40 ± 1.45) × 10^{-4} (1.1)
	G:G	0.41 ± 0.04	1325 ± 249	(3.09 ± 0.64) × 10^{-4}	(9.42 ± 2.42) × 10^{-5} (1.8)
	G:A	0.013 ± 0.001	5516 ± 1061	(2.28 ± 0.47) × 10^{-6}	(6.95 ± 1.78) × 10^{-7} (1.4)
O_5M	G:C	23.5 ± 1.4	9.1 ± 1.9	2.57 ± 0.55	
	G:T	6.08 ± 0.38	3249 ± 445	(1.87 ± 0.28) × 10^{-3}	(7.28 ± 1.90) × 10^{-4} (0.8)
	G:G	0.57 ± 0.05	1003 ± 211	(5.65 ± 1.27) × 10^{-4}	(2.19 ± 0.68) × 10^{-4} (0.8)
	G:A	0.029 ± 0.003	7512 ± 1552	(3.91 ± 0.89) × 10^{-6}	(1.52 ± 0.47) × 10^{-6} (0.6)
O_3M_E478Q	G:C	27.7 ± 1.0	12.5 ± 1.6	2.21 ± 0.30	
	G:T	11.1 ± 2.0	7566 ± 2725	(1.47 ± 0.59) × 10^{-3}	(6.65 ± 2.81) × 10^{-4} (0.9)
	G:G	0.54 ± 0.01	489 ± 16	(1.10 ± 0.04) × 10^{-3}	(4.97 ± 0.70) × 10^{-4} (0.4)
	G:A	0.029 ± 0.002	6362 ± 1110	(4.54 ± 0.86) × 10^{-6}	(2.05 ± 0.48) × 10^{-6} (0.5)
O_3M_T69SSG	G:C	21.1 ± 1.8	14.0 ± 4.4	1.51 ± 0.49	
	G:T	3.15 ± 0.36	4632 ± 1070	(6.80 ± 1.75) × 10^{-4}	(4.50 ± 1.86) × 10^{-4} (1.3)
	G:G	0.26 ± 0.01	2080 ± 250	(1.23 ± 0.16) × 10^{-4}	(8.14 ± 2.85) × 10^{-5} (2.1)
	G:A	(7.6 ± 1.6) × 10^{-3}	5854 ± 1877	(1.30 ± 0.50) × 10^{-6}	(8.61 ± 4.33) × 10^{-7} (1.1)

[a]Oligonucleotides 31T (5′-TTTTTTTTTAGGATACATATGGTTAAAGTAT-3′) and 21P (5′-ATACTTTAACCATATGTATCC-3′) were used as template and primer, respectively. Mismatched extension reactions were conducted with derivatives of 21P having T, G, or A at their 3′ ends. Reported data are means ± the standard deviation. Each of the assays was performed independently at least three times. [b]The first base corresponds to the template and the second to the primer. [c]f_{ext} = [k_{pol}(mismatched)/K_d(mismatched)]/[k_{pol}(matched)/K_d(matched)]. Numbers in parentheses represent the relative increase in fidelity, as determined for each mispair as the f_{ext}(O_WT RT)/f_{ext}(mutant RT) ratio.

O_3M_T69SSG) also showed high affinity for the template-primer, with K_d values of <2 nM. In contrast, destabilizing mutations such as F61A or K65R/E478Q produced a 4−5-fold decrease in binding affinity in comparison with that of the O_3M mutant.

Mutant RTs with Increased Catalytic Efficiency at High Temperatures Show Similar DNA Synthesis Accuracy in Comparison with That of the WT Enzyme. We used gel-based and forward mutation assays to determine the accuracy of RTs showing the highest efficiency above 68 °C. It has been previously shown that RTs are prone to the extension of mispaired template-primers.[17] Therefore, differences in fidelity are more easily detected by using mispair extension fidelity assays. Under pre-steady-state conditions, we determined the kinetic parameters [k_{pol} (pol is polymerization) and K_d] for the incorporation of dTTP opposite A at the 3′ end of the primer, using template-primer duplexes containing matched (G:C) or mismatched 3′ ends (G:T, G:G, and G:A). The comparison of mismatch extension ratios (f_{ext}) of mutants O_3M, O_5M, O_3M_E478Q, and O_3M_T69SSG and the O_WT enzyme revealed only minor differences between the tested enzymes (Table 2). All of the enzymes showed similar catalytic efficiencies of nucleotide incorporation on correctly matched template-primers. In comparison with the O_WT enzyme, O_3M RT showed a reduced catalytic rate (k_{pol}) of dTTP incorporation but an increased nucleotide affinity. This behavior was previously observed for the K65R mutant.[20] However, other RTs having the three substitutions in the connection subdomain (i.e., O_3M_E478Q, O_3M_T69SSG, and O_5M RTs) showed kinetics of nucleotide incorporation similar to those of the WT enzyme, suggesting that subtle changes in the connection subdomain could have a long-range effect on nucleotide incorporation. On the other hand, the O_3M_T69SSG RT showed reduced k_{pol} values in comparison with that of the O_WT enzyme for all tested pairs. Interestingly, the O_3M_T69SSG mutant (together with O_3M RT) was ∼2-fold less efficient than the O_WT RT in extending G:G mispairs. In contrast, the O_3M_E478Q RT was more prone to the extension of G:G and G:A mispairs. Taken together, kinetic studies suggested minor effects of the 3M cluster of mutations on the fidelity of the RT.

The results of the forward mutation assays were consistent with fidelity estimates based on nucleotide incorporation kinetics. Forward mutation assays are based on the detection of mutations generated when the RT copies the gapped region of the *lacZ* gene in the M13mp2 DNA. The corresponding mutants can be detected by a specific indicator strain (and in the presence of IPTG and X-Gal) as plaques with an altered color phenotype (pale blue or colorless). These assays provide a fidelity assessment based on a relatively large number of mutational target sites.[39] In these assays, mutants O_3M, O_3M_E478Q, and O_3M_T69SSG RTs showed similar or higher fidelity than that of the WT HIV-1_O RT (Table 3). Interestingly, the mutant containing the insertion (O_3M_T69SSG RT) showed the highest fidelity, with a mutant frequency of 5.5 × 10^{-3}, approximately 2−3 times lower than the estimates obtained for the HIV-1_O and WT HIV-$1_{M/B/BH10}$ RTs.

DISCUSSION

In previous studies, we showed that WT HIV-1_O RT had a stability increased compared with that of the prototypic HIV-$1_{M/B}$ BH10 RT.[18,19] Studies with chimeric heterodimers attributed a major role in RT stabilization to the 51 kDa subunit.[19] The comparison of the structure homology model of HIV-1_O RT and the crystal structure of HIV-$1_{M/B}$ RT showed relatively minor differences in the free energy of interaction between p66 and p51. Only the presence of Glu[28] in the 51

dx.doi.org/10.1021/bi401390x | Biochemistry 2013, 52, 9318−9328

Table 3. Accuracy of RT Variants in M13mp2 *lacZα* Forward Mutation Assays

RT	total no. of plaques	no. of mutant plaques	mutant frequency[a]	fidelity (*x*-fold increase) (relative to that of O_WT RT)
O_WT[b]				
experiment 1	7579	63	0.00831	
experiment 2	3957	38	0.00960	
O_3M	8394	74	0.00881	1.0
O_3M_E478Q	7802	52	0.00666	1.3
O_3M_T69SSG	14262	79	0.00554	1.6
BH10_WT				
experiment 1	3792	43	0.01134	0.8
experiment 2	2192	29	0.01323	0.7

[a]Reported background frequencies in this assay ($\sim 6 \times 10^{-4}$)[39] are in most cases a consequence of M13mp2 DNA rearrangements that result in the loss of the *lacZ* gene. Phage DNA was obtained from all mutant plaques, and the sequence of the reporter gene was determined in all cases. No *lac*Z mutations were identified after sequencing phage DNA from more than 20000 plaques obtained from two or three *E. coli* electroporations conducted with a gapped M13mp2 DNA substrate.[20] For each enzyme, mutant plaques were obtained after transfection with the products of four to six gap filling reactions. [b]Reported values for O_WT RT were taken from ref 38.

kDa subunit of the HIV-$1_{M/B}$ RT instead of Lys (as observed in HIV-1_O RT) could contribute to the stabilization of the heterodimer through an electrostatic interaction with Lys^{385} in the 66 kDa subunit of HIV-$1_{M/B}$ RT. Nevertheless, our data revealed that substituting Lys^{28} for Glu in HIV-1_O RT did not affect its cDNA synthesis efficiency over a wide range of temperatures.

While differences between both RTs in terms of heterodimer stabilization are relatively small, the free energies of interaction between RT and the template-primer are substantially smaller for the HIV-1_O RT. According to the refined model of this enzyme, strong interactions between the 51 kDa subunit and the template-primer occur at positions 394 and 395 of p51. These contacts have little relevance in the crystal structure of the HIV-$1_{M/B}$ RT−dsDNA−dTTP complex[24] and support the contribution of p51 to the increase in HIV-1_O RT stability. In addition, the analysis of the free energy interaction matrices of both structures unveiled some remarkable differences at specific locations: (1) stronger interactions of the nucleic acid with Arg^{284} and the Arg^{358}-Gly^{359}-Ala^{360}-His^{361} cluster in the 66 kDa subunit of HIV-$1_{M/B}$ RT and (2) weaker interactions affecting residues Gln^{91}, Asp^{113}, Gln^{357}, Lys^{374}, and Ser^{499}. The strong interactions around the cluster of residues 358−360 of the HIV-$1_{M/B}$ RT result from the establishment of a hydrogen bonding network that affects the template-primer and the side chain of Arg^{358}, together with the polypeptide backbone of the Gly^{359}-Ala^{360} pair.

Sequence differences between both HIV-1 RTs were observed around positions 355−360. The Arg^{358}-Gly^{359}-Ala^{360}-His^{361} amino acid sequence is conserved in HIV-1 group M subtype B isolates (e.g., see GenBank entries K03455, AY173951, AY331295, and AY423387) and is also found in subtype D isolates [e.g., ELI (GenBank entry K03454)] as well as in many B/F recombinants (e.g., GenBank entries AY588970, DQ085871, EU581825, and EU735536). In contrast, the equivalent positions (Lys^{358}-Ala^{359}-Ser^{360}-His^{361}) are conserved in HIV-1 group O isolates [e.g., ANT70 (GenBank entry L20587) and MVP5180 (GenBank entry L20571)] (http://www.hiv.lanl.gov/content/sequence/HIV/mainpage.html). The mutational cluster of residues 358−360 is located at a loop joining β-strand 18 (residues 350−358) and α-helix K (residues 364−382)[44] and is surrounded by highly conserved residues in HIV-1 [i.e., KTGKY (residues 350−354) and HRND(V/I) (residues 361−365)]. Reconfiguration of the loops between β-strand 18 and α-helix K and between α-helices B′ and D′ (residues 509−514) is required to accommodate RNA−DNA hybrids containing a widened major groove,[45] and the conformational changes involved may also have a critical impact on the equilibrium of the RT between structural states competent for DNA polymerization and RNA degradation. Crystallographic studies of HIV-$1_{M/B}$ RT in complex with a polypurine tract RNA−DNA complex revealed that Gly^{359}, Ala^{360}, and His^{361} are part of a structure known as the "RNase H primer grip" that helps to determine the trajectory of the template strand relative to the RNase H active site.[46]

By introducing the relevant amino acid changes (i.e., K358R/A359G/S360A) into the HIV-1_O RT, we obtained a mutant polymerase with 3-fold increased DNA binding affinity. The modeling studies suggest that the observed increase is a consequence of a tighter interaction between Arg^{358} and the major groove of the DNA, because of extensive hydrogen bonding interactions. Available studies with RNase H-deficient MLV RTs showed that those enzymes had increased thermal stability in the presence of the template-primer.[11,47] Screening of random libraries of MLV RT variants selected for enzymes with increased resistance to thermal inactivation and tighter binding to template-primers.[14] Our results are consistent with those reports, because above 71 °C, the K358R/A359G/S360A RT showed increased cDNA synthesis efficiency. These observations were corroborated by qPCR. However, further increases in cDNA yields were not observed in reactions catalyzed by mutant RTs carrying additional substitutions at positions 355 and 357. The RNase H-inactivating mutation E478Q had a minimal effect on cDNA yields at temperatures in the range from 50 to 78 °C, in agreement with our previous reports showing that E478Q alone or in combination with V75I had no effect on the thermal stability of WT HIV-1_O RT.[18]

The WT HIV-1_O RT is more faithful than the prototypic WT_BH10 RT,[18] but it is approximately 6−7-fold less faithful than MLV RTs,[21,38] as estimated in M13mp2-based forward mutation assays. The accuracy of HIV-1_O RT was not affected by mutations of residues 358−360. Several amino acid substitutions that increased fidelity in different sequence contexts (e.g., HIV-$1_{M/B}$ and HIV-1_O) were tested in combination with the complex of residues 358−360. Addition of K65R resulted in RTs with higher fidelity in elongation assays conducted in the presence of three dNTPs (data not shown). However, O_3M RTs bearing mutation K65R, double mutation K65R/V75I, or double mutation K65R/E478Q had reduced cDNA synthesis efficiencies above 65 °C that correlated with their reduced DNA binding affinity. There is no clear structural explanation for those differences, although K65R could have some indirect effect on the positioning of the template-primer that would reduce its binding affinity. The most dramatic decreases in catalytic efficiency at high temperatures were observed after the addition of mutations F61A or V148I. The DNA binding affinity of the O_3M_F61A mutant was ∼6-fold reduced compared with that of the O_3M RT and lower than that obtained with the WT HIV-1_O RT. In agreement with our results, Phe^{61} (together with Trp^{24}) was previously described as an important residue for template-

dx.doi.org/10.1021/bi401390x | *Biochemistry* 2013, 52, 9318−9328

primer binding[48] and heterodimer stability.[49] On the other hand, adding the T69S mutation together with the insertion of Ser-Gly (T69SSG) to the K358R/A359G/S360A RT maintained the DNA binding and catalytic efficiency properties of the enzyme. Interestingly, the resulting RT showed increased fidelity in forward mutation assays, although the effects were less pronounced than those reported for the same insertion complex when it was added to a WT HIV-$1_{M/B}$ RT.[43]

Interestingly, clinical studies have shown that RT mutations in HIV-$1_{M/B}$ isolates such as R358K,[50] G359S,[50,51] or A360T and A360V[50−54] are more prevalent in patients treated with nucleoside analogues, particularly with zidovudine. Although the biochemical consequences of those mutations are subtle, it is clear that their influence on template-primer binding affects the equilibrium between nucleotide excision and RNase H activity that are major factors contributing to drug resistance.[55,56]

In summary, our study demonstrates that the loop between β-strand 18 and α-helix K is a major target for the stabilization of RTs and more specifically the mutations of the Arg^{358}-Gly^{359}-Ala^{360} triad (or its equivalent in the RTs of other HIV clades) that play a critical role in template-primer binding. Stabilized enzymes showed increased DNA synthesis efficiency at high temperatures. However, fidelity emerges as an independent property, because mutations that increase the accuracy of DNA synthesis in a WT sequence context do not exert the same effects when the connection subdomain mutations are present in the corresponding RT.

■ ASSOCIATED CONTENT

Supporting Information

Table of primers used to construct the mutants (Table S1), figures showing the analysis of interactions between p66 and p51 and between RTs and template-primers (Figures S1−3), and figures describing the effect of temperature in RT-PCRs and real-time PCR amplifications (Figures S4 and S5). This material is available free of charge via the Internet at http://pubs.acs.org.

■ AUTHOR INFORMATION

Corresponding Author

*Centro de Biología Molecular "Severo Ochoa" (CSIC-UAM), c/Nicolás Cabrera 1, Campus de Cantoblanco, 28049 Madrid, Spain. Telephone: +34 91 196 4494. Fax: +34 91 196 4420. E-mail: lmenendez@cbm.uam.es.

Funding

This work was supported by grants from the Spanish Ministries of Economy and Competitiveness (BIO2010/15542) and Health, Social Services and Equality (EC11-025) and an institutional grant to the CBMSO from the Fundación Ramón Areces.

Notes

A provisional patent covering thermostable RTs containing the described connection subdomain mutations has been filed by the Consejo Superior de Investigaciones Científicas with all authors participating as co-inventors.

■ ACKNOWLEDGMENTS

We thank Mireya Rodrigo for technical assistance with forward mutation assays.

■ ABBREVIATIONS

AMV, avian myeloblastosis virus; cDNA, complementary DNA; C_T, threshold cycle; dsDNA, double-stranded DNA; GAPDH, glyceraldehyde-3-phosphate dehydrogenase; GB, generalized Born; MLV, murine leukemia virus; MM, molecular mechanics; qPCR, quantitative polymerase chain reaction; RT, reverse transcriptase; RT-PCR, reverse transcription polymerase chain reaction; SA, surface area; SASA, solvent accessible surface area; WT, wild-type; XMRV, xenotropic murine leukemia virus-related virus.

■ REFERENCES

(1) Herschhorn, A., and Hizi, A. (2010) Retroviral reverse transcriptases. *Cell. Mol. Life Sci. 67*, 2717−2747.

(2) Matamoros, T., Álvarez, M., Barrioluengo, V., Betancor, G., and Menéndez-Arias, L. (2011) Reverse transcriptase and retroviral replication. In *DNA replication and related cellular process* (Kušić-Tišma, J., Ed.) pp 111−142, InTech, Rijeka, Croatia.

(3) Winter, H., Korn, K., and Rigler, R. (2004) Direct gene expression analysis. *Curr. Pharm. Biotechnol. 5*, 191−197.

(4) Wong, M. L., and Medrano, J. F. (2005) Real-time PCR for mRNA quantitation. *BioTechniques 39*, 75−85.

(5) Ozsolak, F., and Milos, P. M. (2011) RNA sequencing: Advances, challenges and opportunities. *Nat. Rev. Genet. 12*, 87−98.

(6) Lovén, J., Orlando, D. A., Sigova, A. A., Lin, C. Y., Rahl, P. B., Burge, C. B., Levens, D. L., Lee, T. I., and Young, R. A. (2012) Revisiting global gene expression analysis. *Cell 151*, 476−482.

(7) Mohr, S., Ghanem, E., Smith, W., Sheeter, D., Qin, Y., King, O., Polioudakis, D., Iyer, V. R., Hunicke-Smith, S., Swamy, S., Kuersten, S., and Lambowitz, A. M. (2013) Thermostable group II intron reverse transcriptase fusion proteins and their use in cDNA synthesis and next-generation RNA sequencing. *RNA 19*, 958−970.

(8) Harrison, G. P., Mayo, M. S., Hunter, E., and Lever, A. M. (1998) Pausing of reverse transcriptase on retroviral RNA templates is influenced by secondary structures both 5′ and 3′ of the catalytic site. *Nucleic Acids Res. 26*, 3433−3442.

(9) Klasens, B. I., Huthoff, H. T., Das, A. T., Jeeninga, R. E., and Berkhout, B. (1999) The effect of template RNA structure on elongation by HIV-1 reverse transcriptase. *Biochim. Biophys. Acta 1444*, 355−370.

(10) Ståhlberg, A., Kubista, M., and Pfaffl, M. (2004) Comparison of reverse transcriptases in gene expression analysis. *Clin. Chem. 50*, 1678−1680.

(11) Gerard, G. F., Potter, R. J., Smith, M. D., Rosenthal, K., Dhariwal, G., Lee, J., and Chatterjee, D. K. (2002) The role of template-primer in protection of reverse transcriptase from thermal inactivation. *Nucleic Acids Res. 30*, 3118−3129.

(12) Yasukawa, K., Mizuno, M., Konishi, A., and Inouye, K. (2010) Increase in thermal stability of Moloney murine leukaemia virus reverse transcriptase by site-directed mutagenesis. *J. Biotechnol. 150*, 299−306.

(13) Konishi, A., Yasukawa, K., and Inouye, K. (2012) Improving the thermal stability of avian myeloblastosis virus reverse transcriptase α-subunit by site-directed mutagenesis. *Biotechnol. Lett. 34*, 1209−1215.

(14) Arezi, B., and Hogrefe, H. (2009) Novel mutations in Moloney murine leukemia virus reverse transcriptase increase thermostability through tighter binding to template-primer. *Nucleic Acids Res. 37*, 473−481.

(15) Baranauskas, A., Paliksa, S., Alzbutas, G., Vaitkevicius, M., Lubiene, J., Letukiene, V., Burinskas, S., Sasnauskas, G., and Skirgaila, R. (2012) Generation and characterization of new highly thermostable and processive M-MuLV reverse transcriptase variants. *Protein Eng. Des. Sel. 25*, 657−668.

(16) Nowak, E., Potrzebowski, W., Konarev, P. V., Rausch, J. W., Bona, M. K., Svergun, D. I., Bujnicki, J. M., Le Grice, S. F. J., and Nowotny, M. (2013) Structural analysis of monomeric retroviral

reverse transcriptase in complex with an RNA/DNA hybrid. *Nucleic Acids Res. 41*, 3874−3887.
(17) Menéndez-Arias, L. (2009) Mutation rates and intrinsic fidelity of retroviral reverse transcriptases. *Viruses 1*, 1137−1165.
(18) Álvarez, M., Matamoros, T., and Menéndez-Arias, L. (2009) Increased thermostability and fidelity of DNA synthesis of wild-type and mutant HIV-1 group O reverse transcriptases. *J. Mol. Biol. 392*, 872−884.
(19) Menéndez-Arias, L., Abraha, A., Quiñones-Mateu, M. E., Mas, A., Camarasa, M.-J., and Arts, E. J. (2001) Functional characterization of chimeric reverse transcriptases with polypeptide subunits of highly divergent HIV-1 group M and O strains. *J. Biol. Chem. 276*, 27470−27479.
(20) Barrioluengo, V., Álvarez, M., Barbieri, D., and Menéndez-Arias, L. (2011) Thermostable HIV-1 group O reverse transcriptase variants with the same fidelity as murine leukaemia virus reverse transcriptase. *Biochem. J. 436*, 599−607.
(21) Barrioluengo, V., Wang, Y., Le Grice, S. F. J., and Menéndez-Arias, L. (2012) Intrinsic DNA synthesis fidelity of xenotropic murine leukemia virus-related virus reverse transcriptase. *FEBS J. 279*, 1433−1444.
(22) Roberts, J. D., Bebenek, K., and Kunkel, T. A. (1988) The accuracy of reverse transcriptase from HIV-1. *Science 242*, 1171−1173.
(23) Roberts, J. D., Preston, B. D., Johnston, L. A., Soni, A., Loeb, L. A., and Kunkel, T. A. (1989) Fidelity of two retroviral reverse transcriptases during DNA-dependent DNA synthesis in vitro. *Mol. Cell. Biol. 9*, 469−476.
(24) Huang, H., Chopra, R., Verdine, G., and Harrison, S. (1998) Structure of a covalently trapped catalytic complex of HIV-1 reverse transcriptase: Implications for drug resistance. *Science 282*, 1669−1675.
(25) Eswar, N., Webb, B., Marti-Renom, M. A., Madhusudhan, M. S., Eramian, D., Shen, M. Y., Pieper, U., and Sali, A. (2006) Comparative protein structure modeling using Modeller. *Current Protocols in Bioinformatics*, Chapter 5, Unit 5.6, Wiley, New York.
(26) Ryckaert, J.-P., Ciccotti, G., and Berendsen, H. J. C. (1977) Numerical integration of the cartesian equations of motion of a system with constraints: Molecular dynamics of n-alkanes. *J. Comput. Phys. 23*, 327−341.
(27) Darden, T., York, D., and Pedersen, L. (1993) Particle mesh Ewald: An $N\cdot\log(N)$ method for Ewald sums in large systems. *J. Chem. Phys. 98*, 10089−10092.
(28) Duan, Y., Wu, C., Chowdhury, S., Lee, M. C., Xiong, G., Zhang, W., Yang, R., Cieplak, P., Luo, R., Lee, T., Caldwell, J., Wang, J., and Kollman, P. (2003) A point-charge force field for molecular mechanics simulations of proteins based on condensed-phase quantum mechanical calculations. *J. Comput. Chem. 24*, 1999−2012.
(29) Jorgensen, W. L., Chandrasekhar, J., Madura, J. D., Impey, R. W., and Klein, M. L. (1983) Comparison of simple potential functions for simulating liquid water. *J. Chem. Phys. 79*, 926−935.
(30) Still, W. C., Tempczyk, A., Hawley, R. C., and Hendrickson, T. (1990) Semianalytical treatment of solvation for molecular mechanics and dynamics. *J. Am. Chem. Soc. 112*, 6127−6129.
(31) Case, D. A., Darden, T. A., Cheatham, T. E., III, Simmerling, C. L., Wang, J., Duke, R. E., Luo, R., Crowley, M., Walker, R. C., Zhang, W., Merz, K. M., Wang, B., Hayik, S., Roitberg, A., Seabra, G., Kolossváry, I., Wong, K. F., Paesani, F., Vanicek, J., Wu, X., Brozell, S. R., Steinbrecher, T., Gohlke, H., Yang, L., Tan, C., Mongan, J., Hornak, V., Cui, G., Mathews, D. H., Seetin, M. G., Sagui, C., Babin, V., and Kollman, P. A. (2008) *AMBER 10*, University of California, San Francisco.
(32) Pavlidis, P., and Noble, W. S. (2003) Matrix2png: A utility for visualizing matrix data. *Bioinformatics 19*, 295−296.
(33) Boretto, J., Longhi, S., Navarro, J.-M., Selmi, B., Sire, J., and Canard, B. (2001) An integrated system to study multiply substituted human immunodeficiency virus type 1 reverse transcriptase. *Anal. Biochem. 292*, 139−147.
(34) Kati, W. M., Johnson, K. A., Jerva, L. F., and Anderson, K. S. (1992) Mechanism and fidelity of HIV reverse transcriptase. *J. Biol. Chem. 267*, 25988−25997.
(35) Schmittgen, T. D., and Livak, K. J. (2008) Analyzing real-time PCR data by the comparative C_T method. *Nat. Protoc. 3*, 1101−1108.
(36) Betancor, G., Puertas, M. C., Nevot, M., Garriga, C., Martínez, M. A., Martinez-Picado, J., and Menéndez-Arias, L. (2010) Mechanisms involved in the selection of HIV-1 reverse transcriptase thumb subdomain polymorphisms associated with nucleoside analogue therapy failure. *Antimicrob. Agents Chemother. 54*, 4799−4811.
(37) Menéndez-Arias, L. (1998) Studies on the effects of truncating α-helix E′ of p66 human immunodeficiency virus type 1 reverse transcriptase on template-primer binding and fidelity of DNA synthesis. *Biochemistry 37*, 16636−16644.
(38) Álvarez, M., Barrioluengo, V., Afonso-Lehmann, R., and Menéndez-Arias, L. (2013) Altered error specificity of RNase H-deficient HIV-1 reverse transcriptases during DNA-dependent DNA synthesis. *Nucleic Acids Res. 41*, 4601−4612.
(39) Bebenek, K., and Kunkel, T. A. (1995) Analyzing fidelity of DNA polymerases. *Methods Enzymol. 262*, 217−232.
(40) Fisher, T. S., and Prasad, V. R. (2002) Substitutions of Phe^{61} located in the vicinity of template 5′-overhang influence polymerase fidelity and nucleoside analog sensitivity of HIV-1 reverse transcriptase. *J. Biol. Chem. 277*, 22345−22352.
(41) Diamond, T. L., Souroullas, G., Weiss, K. K., Lee, K. Y., Bambara, R. A., Dewhurst, S., and Kim, B. (2003) Mechanistic understanding of an altered fidelity simian immunodeficiency virus reverse transcriptase mutation, V148I, identified in a pig-tailed macaque. *J. Biol. Chem. 278*, 29913−29924.
(42) Weiss, K. K., Chen, R., Skasko, M., Reynolds, H. M., Lee, K., Bambara, R. A., Mansky, L. M., and Kim, B. (2004) A role for dNTP binding of human immunodeficiency virus type 1 reverse transcriptase in viral mutagenesis. *Biochemistry 43*, 4490−4500.
(43) Curr, K., Tripathi, S., Lennerstrand, J., Larder, B. A., and Prasad, V. R. (2006) Influence of naturally occurring insertions in the fingers subdomain of human immunodeficiency virus type 1 reverse transcriptase on polymerase fidelity and mutation frequencies *in vitro*. *J. Gen. Virol. 87*, 419−428.
(44) Lapkouski, M., Tian, L., Miller, J. T., Le Grice, S. F. J., and Yang, W. (2013) Complexes of HIV-1 RT, NNRTI and RNA/DNA hybrid reveal a structure compatible with RNA degradation. *Nat. Struct. Mol. Biol. 20*, 230−236.
(45) Jacobo-Molina, A., Ding, J., Nanni, R., Clark, A., Lu, X., Tantillo, C., Williams, R., Kamer, G., Ferris, A., Clark, P., Hizi, A., Hughes, S., and Arnold, E. (1993) Crystal structure of human immunodefiency virus type 1 reverse transcriptase complexed with double-stranded DNA at 3.0 Å resolution shows bent DNA. *Proc. Natl. Acad. Sci. U.S.A. 90*, 6320−6324.
(46) Sarafianos, S. G., Das, K., Tantillo, C., Clark, A. D., Jr., Ding, J., Whitcomb, J. M., Boyer, P. L., Hughes, S. H., and Arnold, E. (2001) Crystal structure of HIV-1 reverse transcriptase in complex with a polypurine tract RNA:DNA. *EMBO J. 20*, 1449−1461.
(47) Pinto, F. L., and Lindblad, P. (2010) A guide for in-house design of template-switch-based 5′ rapid amplification of cDNA ends systems. *Anal. Biochem. 397*, 227−232.
(48) Agopian, A., Depollier, J., Lionne, C., and Divita, G. (2007) p66 Trp24 and Phe61 are essential for accurate association of HIV-1 reverse transcriptase with primer/template. *J. Mol. Biol. 373*, 127−140.
(49) Depollier, J., Hourdou, M. L., Aldrian-Herrada, G., Rothwell, P., Restle, T., and Divita, G. (2005) Insight into the mechanism of a peptide inhibitor of HIV reverse transcriptase dimerization. *Biochemistry 44*, 1909−1918.
(50) Lengruber, R. B., Delviks-Frankenberry, K. A., Nikolenko, G. N., Baumann, J., Santos, A. F., Pathak, V. K., and Soares, M. A. (2011) Phenotypic characterization of drug resistance-associated mutations in HIV-1 RT connection and RNase H domains and their correlation with thymidine analogue mutations. *J. Antimicrob. Chemother. 66*, 702−708.

(51) Cane, P. A., Green, H., Fearnhill, E., and Dunn, D. on behalf of the UK collaborative group on HIV Drug Resistance (2007) Identification of accessory mutations associated with high-level resistance in HIV-1 reverse transcriptase. *AIDS 21*, 447−455.
(52) Ehteshami, M., Beilhartz, G. L., Scarth, B. J., Tchesnokov, E. P., McCormick, S., Wynhoven, B., Harrigan, P. R., and Götte, M. (2008) Connection domain mutations N348I and A360V in HIV-1 reverse transcriptase enhance resistance to 3′-azido-3′-deoxythymidine through both RNase H-dependent and -independent mechanisms. *J. Biol. Chem. 283*, 22222−22232.
(53) Santos, A. F., Lengruber, R. B., Soares, E. A., Jere, A., Sprinz, E., Martinez, A. M., Silveira, J., Sion, F. S., Pathak, V. K., and Soares, M. A. (2008) Conservation patterns of HIV-1 RT connection and RNase H domains: Identification of new mutations in NRTI-treated patients. *PLoS One 3*, e1781.
(54) Brehm, J. H., Scott, Y., Koontz, D. L., Perry, S., Hammer, S., Katzenstein, D., Mellors, J. W., Sluis-Cremer, N., and AIDS Clinical Trials Group Study 175 Protocol Team (2012) Zidovudine (AZT) monotherapy selects for the A360V mutation in the connection domain of HIV-1 reverse transcriptase. *PLoS One 7*, e31558.
(55) Nikolenko, G. N., Delviks-Frankenberry, K. A., Palmer, S., Maldarelli, F., Fivash, M. J., Jr., Coffin, J. M., and Pathak, V. K. (2007) Mutations in the connection domain of HIV-1 reverse transcriptase increase 3′-azido-3′-deoxythymidine resistance. *Proc. Natl. Acad. Sci. U.S.A. 104*, 317−322.
(56) Menéndez-Arias, L. (2013) Molecular basis of human immunodeficiency virus type 1 drug resistance: Overview and recent developments. *Antiviral Res. 98*, 93−120.